

# Propagation and Filamentation of Femtosecond Laser Pulses in Optical Media<sup>1</sup>

N. Aközbek<sup>1</sup>, A. Becker<sup>2,\*</sup>, and S. L. Chin<sup>3</sup>

<sup>1</sup> Time Domain Corporation, 7057 Old Madison Pike, Huntsville, AL 35806, USA

<sup>2</sup> Max-Planck-Institut für Physik komplexer Systeme, Nöthnitzer Str. 38, D-01187 Dresden, Germany

\*e-mail: abecker@mpipks-dresden.mpg.de

<sup>3</sup> Département de Physique, de Génie Physique et d’Optique and Centre d’Optique, Photonique et Laser, Université Laval, Québec, G1K7P4, Canada

Received October 27, 2004

**Abstract**—We discuss our recent results on the propagation dynamics of high-peak-power femtosecond laser pulses in optical media. A number of important nonlinear effects, such as white-light continuum generation, intensity clamping, transverse ring formation, and third-harmonic generation, are presented. It is shown that the self-steepening of the pulse has an important role in supercontinuum generation and cannot be neglected. When laser pulse filamentation takes place, it is found both experimentally and theoretically that the peak pulse intensity is clamped down, which is an universal phenomenon in gases, liquids, and condensed matter. Theoretical and experimental results on the formation of transverse rings are presented, which exhibit the rich dynamics of femtosecond-pulse propagation. Finally, we show that an intense third-harmonic pulse is generated and undergoes filamentation together with the pump pulse. This is found to be a consequence of a nonlinear phase-locking mechanism between the two pulses that results in two-colored filament formation.

*A Tribute to Dr. Charles Malcolm Bowden*

Before we start discussing the science, we would like to pay our most sincere respect to the late Dr. Charles Bowden (we all know him as Chuck), who was co-organizer of Seminar 5 of the annual Laser Physics workshop for many years. The subject matter in this paper has a deep relationship with Chuck’s initiative, his leadership, and his deep insight and foresightedness concerning the subject.

In 1996, after one of us (SLC) presented a talk on long-distance filamentation of femtosecond laser pulses in the atmosphere at an international conference in Moscow, Chuck approached him and discussed collaboration. Chuck foresaw immediately that there would be many interesting and challenging physics and applications in this new subject of endeavor. These include intense-field physics, extreme nonlinear optics, nonlinear electromagnetic pulse propagation, quantum optics, and some unknown new physical phenomena. Since then, the very fruitful collaboration between his group and us has resulted in more than a dozen joint publications in prestigious international scientific journals. This collaboration has led to the fundamental understanding of many physical aspects of the self-focusing, filamentation, and consequences during the propagation of femtosecond laser pulses. Some of these constitute the subject matter of this paper.

The impact of Chuck on his friends and fellow scientists cannot be totally expressed. We would just like to touch upon it through the following poem composed

by one of us (SLC) on behalf of all his collaborators in the field of ultrafast intense laser science. It was read during the funeral service for Chuck in Huntsville, Alabama, USA on Aug. 17, 2004.

*Dear Chuck*

*We all miss you  
Deep from our heart.  
We remember  
Your youthful action, forever  
Sliding down the icy sugar cone  
At the Montmorency Falls of Quebec City  
Deep in the winter.  
We remember  
Your optimistic view of life  
Enjoying every moment wherever you happened to be  
Across this planet earth.  
We remember  
Your acute scientific judgement and leadership  
Forever pushing the frontier of knowledge  
Advising your superior on the emerging technologies  
Involving so many of us to debate together  
About the truth of science  
In an exciting and friendly atmosphere.  
We remember, in particular  
Your generosity  
Sharing your intellectual wealth  
Helping those in need  
Keeping us all excited and cohesive  
In the world of science.  
We all miss you Chuck.  
Rest well, please.*

<sup>1</sup> This paper is dedicated to Dr. C.M. Bowden, co-organizer of Seminar 5, *Nonlinear Optics and Spectroscopy*, of the annual Laser Physics workshop, who passed away on August 14, 2004.

## 1. INTRODUCTION

The propagation of a high-peak-power femtosecond pulse in transparent condensed media, gases, or air can result in strong modification of its shape by self-focusing and defocusing in the spatial domain and by self-phase modulation in the temporal domain (e.g., [1, 2]). Self-focusing is a dynamical Kerr lens effect, which causes the pulse to be contracted in space [3]. The process is balanced at high enough intensities by defocusing due to the formation of a low-density plasma. While in gases the plasma is generated due to multiphoton ionization (e.g., [4]), in condensed matter quasi-free electrons are created by multiphoton excitation from the valence to the conduction band [5]. The dynamical balance between Kerr self-focusing and plasma defocusing is known to lead to the appearance of filaments in the optical media (e.g., [4]). The long-range propagation of the pulses beyond their first self-focus depends on the use of subpicosecond laser pulses, which are short enough to avoid the occurrence of avalanche ionization. The details of the filamentation process are complex, and different interpretations such as the self-channeling model [4], the moving focus picture [6], or spatial replenishment [7] have been proposed. During the propagation of the pulse self-phase modulation causes a spectral broadening. This phenomenon has been found to appear universally in all optical media, namely, solids [5], liquids [8], gases [9], and air [10], and is named supercontinuum generation or white-light laser [11, 12]. In general, it has been found that, besides self-phase modulation, various other nonlinear effects, such as self-steepening, can contribute to the generation of the white-light spectrum [13].

There has been great interest in the last several years in the propagation of high-peak-power femtosecond laser pulses in optical media due to the wide variety of possible applications, such as optical pulse compression [11], optical parametric amplification [14], time-resolved broadband spectroscopy [11], lightning discharge control [15, 16], and remote sensing [10]. For example, the ability to generate an ultrashort intense white-light source at remote locations has been demonstrated recently for atmospheric remote sensing [17]. Besides these applications the phenomenon of filament formation is also very interesting from a fundamental nonlinear-dynamical point of view. Since temporal and spatial dynamics cannot be separated, theoretical investigations have to involve a number of coupled nonlinear effects. Much progress towards numerical solutions of propagation models based on the Maxwell equations has been made recently in this direction.

In this paper, we discuss some of our recent findings in femtosecond-pulse propagation and filamentation in various optical media. First, we will consider the supercontinuum generation during the propagation of a pulse in air and analyze the influence of self-steepening on the spectrum. Next, we will show that inside the filament the intensity is clamped down to a maximum

value, a phenomenon that appears to be universal for all kinds of optical media. Then the formation of a transverse ring with near-infrared pulses during propagation in air will be discussed and, finally, we will end by showing that in air the filamentation of the pulse is coupled with the generation and filamentation of a strong third-harmonic pulse.

## 2. SUPERCONTINUUM GENERATION AND SELF-STEEPENING

Ultrafast supercontinuum generation has been a subject of interest in nonlinear optics for over 30 years now [11]. It is a result of the propagation of intense subpicosecond laser pulses in bulk transparent media. In most cases the spectral broadening of the pulse can be explained through self-phase modulation. However, in general various other nonlinear effects cannot be neglected and may contribute to the supercontinuum generation. We have analyzed supercontinuum generation in air using a pulse-propagation model that goes beyond the slowly varying envelope approximation [18]. The generalized propagation equation is derived using the approach by Brabec and Krausz [19] and by self-consistently including multiphoton ionization of the air molecules. The model is used here for propagation of pulses in air but can be applied also to propagation in other types of bulk media, including liquids.

The propagation equation can be written in dimensionless form in the retarded coordinate frame ( $\tau = t - z/v_g$ ) as [18]

$$\left\{ i \frac{\partial}{\partial z} + \frac{1}{4} \left( 1 + is \frac{\partial}{\partial \tau} \right)^{-1} \nabla_{\perp}^2 - \frac{1}{4} \frac{L_D}{L_d} \left( \frac{\partial^2}{\partial \tau^2} + \frac{i L_d}{3 L_d'} \frac{\partial^3}{\partial \tau^3} \right) \right\} \mathcal{E} + \frac{L_D}{L_{NL}} \left( 1 + is \frac{\partial}{\partial \tau} \right) F_{NL} \mathcal{E} - \frac{L_D}{L_{\text{plasma}}} \left( 1 + is \frac{\partial}{\partial \tau} \right)^{-1} N_e \mathcal{E} + i \frac{L_D}{L_{MPA}} |\mathcal{E}|^{2n-2} \mathcal{E} = 0, \quad (1)$$

where  $F_{NL} = (1 - \alpha)|\mathcal{E}|^2 + \alpha \int_{-\infty}^{\tau} R(\tau - \tau') |\mathcal{E}|^2 d\tau'$ , and where the generated electron density  $N_e(z, r, \tau)$  is obtained from

$$\frac{\partial N_e}{\partial \tau} = |\mathcal{E}|^{2n}. \quad (2)$$

$\mathcal{E}(z, r, \tau)$  is the electric-field envelope function with  $\mathcal{E}(z=0, r, \tau) = \exp(-(r^2 + \tau^2))$ , where  $\mathcal{E}$  is normalized to the peak input field. The transverse,  $r$ , and temporal,  $\tau$ , coordinates are normalized to the initial beam radius  $w_0$  and the pulse width  $\tau_0$ , respectively. The propagation distance  $z$  is given in units of the diffraction length  $L_D = kw_0^2/2$ , where  $k = n_0 k_0$  and  $n_0$  is the linear index of refraction of air. The dispersion length scales are

defined as  $L_d = \tau_0^2/2k''$  and  $L_d' = \tau_0^3/2k'''$ , where  $k''$  and  $k'''$  are the second- and third-order group-velocity dispersion coefficients, respectively. For air,  $k'' = 0.2 \text{ fs}^2/\text{cm}$  and  $k''' = 0.1 \text{ fs}^3/\text{cm}$  at  $\lambda_0 = 800 \text{ nm}$  [20]. The nonlinear length scale  $L_{NL} = 1/n_2 k_0 I_0$ , where  $n_2 = 4 \times 10^{-19} \text{ cm}^2/\text{W}$  [21] is the nonlinear index of refraction coefficient and  $I_0$  is the input peak intensity given in units of  $\text{W}/\text{cm}^2$ .  $L_D/L_{NL}$  can also be written as  $L_D/L_{NL} = 2P_0/P_{cr}$ , where  $P_0$  is the input power and  $P_{cr} = \lambda_0^2/2\pi n_0 n_2$  is the critical power for self-focusing in the CW limit, which is about 3 GW for air at 800 nm. The Raman response function  $R(\tau)$  accounts for the delayed nonlinear effect and  $\alpha$  denotes the fractional amount of the time-delayed nonlinear response. The generated electron density  $N_e$  is normalized to  $N_0 \tau_0 \sigma^{(n)} I_0^n$ , where  $N_0 = 3 \times 10^{19} \text{ cm}^{-3}$  is the number density of neutral air molecules (20%  $\text{O}_2$  and 80%  $\text{N}_2$ ) and  $\sigma^{(n)}$  is the ionization cross section. The ionization rate is obtained by fitting the experimental data to the form of  $\sigma^{(n)} I^n$ , where  $n = 6-7$ . The plasma length scale is defined as  $L_{\text{plasma}} = km_e c^2/2\pi e^2 \tau_0 N_0 \sigma^{(n)} I_0^n$ , and  $L_{MPA} = n\hbar\omega_0 N_0 \sigma^{(n)} I_0^{n-1}/2$  is the length scale for multiphoton absorption due to ionization losses. The parameter  $s = 1/\omega_0 \tau_0$  represents an expansion coefficient associated with the higher order correction terms to the nonlinear Schrödinger equation in the slowly varying envelope approximation.

We have integrated Eqs. (1) and (2) for the following initial conditions:  $\tau_0 = 127.5 \text{ fs}$  (150 fs FWHM) and  $w_0 = 250 \mu\text{m}$ , so that  $L_D/L_{\text{plasma}} = 9 \times 10^{-2}$  and  $P_0/P_{cr} = 6$ . We define the spectral density as  $S(r, \omega) = |E(r, \omega)|^2$ , from which the average spectrum is obtained by  $S(\omega) = 2\pi \int_0^{r_{\text{filament}}} |E(r, \omega)|^2 r dr$ , where  $r_{\text{filament}} = 0.3$  (in units of the input beam radius) is chosen such that the significant portion of the filament is taken into account.  $L_D/L_d = 0.05$ ,  $L_d/L_d' = 0.005$ , and  $s = 1/\omega_0 \tau_0 = 0.005$ .

In Fig. 1 the effect of higher order correction terms ( $s \neq 0$ ) in Eq. (1) on the power spectrum is investigated. The spectrum at a propagation distance  $z = 1.0$  obtained with the generalized equation (dashed-and-dotted line) is compared with the result obtained by the slowly varying envelope approximation ( $s = 0$ ) (dotted line). The initial pulse spectrum is also shown for reference (solid line). It is clearly seen from this comparison that the inclusion of higher order terms, in particular the self-steepening term (time derivative of the nonlinear index), causes a strong blueshift. At further propagation distances, the spectrum develops a smooth shoulder on the blue side of the spectrum, as depicted in Fig. 2. The main reason for the strong blueshift is a shock formation at the back of the pulse, shown in Fig. 3. This spectrum is in good qualitative agreement with the experimentally observed white-light continuum in air [10].

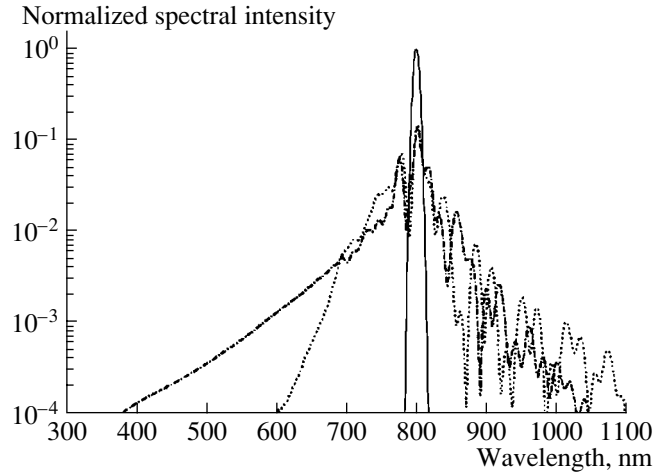


**Fig. 1.** Compared are the power spectra of the optical pulse at a propagation distance of  $z = 1.0$  (in units of diffraction length) in the case of SVEA (dotted line) and non-SVEA (dotted-and-dashed line). The solid curve is the initial pulse spectrum at  $z = 0$ . It is clearly seen that higher order terms in Eq. (1) contribute significantly to the blue side of the spectrum as compared to the SVEA case. The spectral intensities are normalized to the peak input spectral intensity.

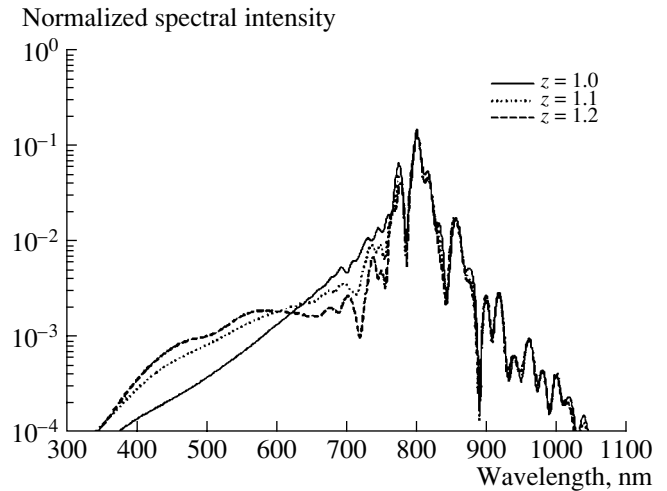


**Fig. 2.** The simulated power spectrum using the non-SVEA wave equation ( $s = 0.005$ ) is plotted for  $z = 1.0$  (solid line),  $z = 1.1$  (dotted line), and  $z = 1.2$  (dashed line).

### 3. INTENSITY CLAMPING

It is difficult to investigate the properties of laser filaments, such as their temporal and spatial intensity distribution, experimentally, since the peak intensity within the filaments far exceeds the damage threshold of any measurement system. Alternatively, information must be determined by observations outside the interaction volume. We have performed two kinds of experiments [22, 27] to show that the peak intensity in laser

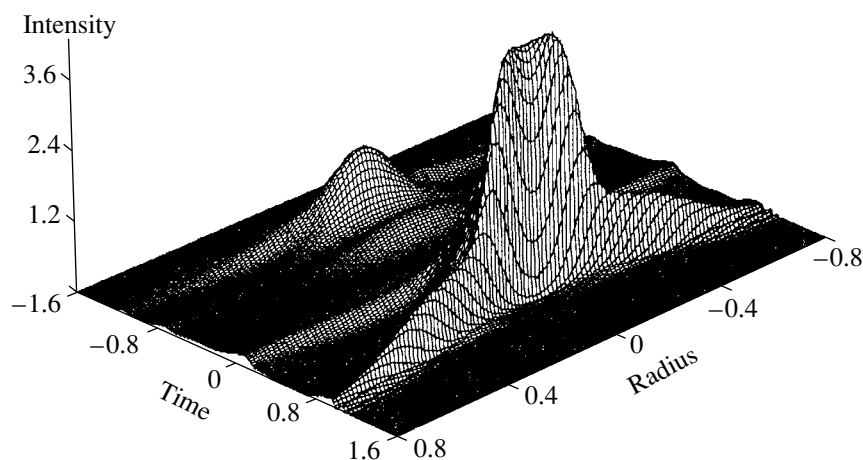


**Fig. 3.** The spatio-temporal intensity profile is plotted with all higher order terms included at a propagation distance of  $z = 1.0$ . Notice the steep edge at the back of the pulse, which causes the strong blueshifted spectrum depicted in Fig. 1 (dotted-and-dashed line).

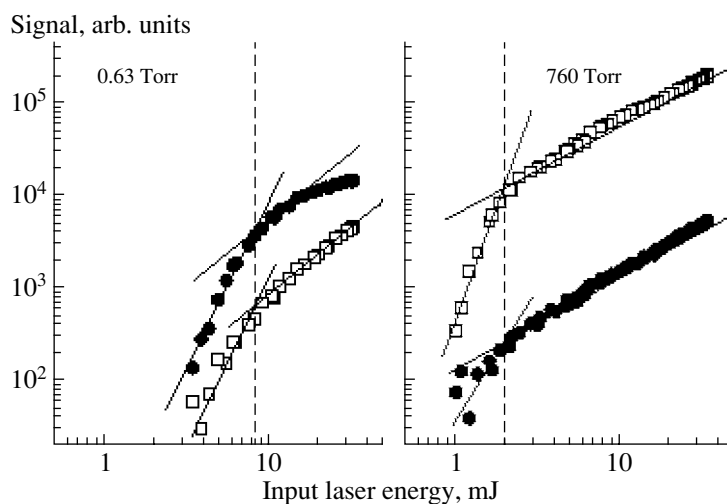


**Fig. 4.** Comparison of the intensities of the strongest band heads of the second positive band system in  $N_2$  (open squares) and of the first negative band system in  $N_2^+$  (closed circles) at low (left-hand panel) and atmospheric pressures (right-hand panel) as a function of the laser energy.

filaments in any optical medium is clamped down to a maximum value. In nitrogen gases, we have observed the fluorescence spectra of the nitrogen molecule and molecular ion at different gas pressures [22], while, in condensed media, the supercontinuum spectrum of the self-transformed laser pulse is measured [27].

### 3.1. Intensity Clamping in Nitrogen Molecular Gas

For the fluorescence measurements from laser pulse filaments, the beam of a Ti:sapphire laser system, delivering pulses at 800 nm and 250 fs, was focused through a 100-cm lens in an interaction chamber filled with nitrogen molecular gas. At high gas pressures and high input energies, a filament occurred around the geomet-

rical focus, which was imaged onto the center of the entrance of the spectrometer. Further details of the experimental setup can be found in [22, 23]. In Fig. 4, the results of our observations for the strongest band heads in a neutral nitrogen molecule (open squares) and in the molecular ion (closed circles) are plotted as a function of the input pulse energy [22]. The data are obtained at 0.63 Torr (left-hand panel) and atmospheric pressure (right-hand panel). The fluorescence signal at both pressures shows a quick rise when the laser energy is increased, followed by a characteristic change of slope towards a slower increase. The change of slope is found to appear at the same input energy for both the band heads. It is seen from the comparison in Fig. 4 that this energy is smaller at atmospheric pressure than at

low pressure. We may note that, at the higher pressure, a filament was observed for input energies larger than the energy at which the change of slope occurs.

Since excitation and ionization of atoms and molecules in intense laser pulses are highly nonlinear processes, the fluorescence signals in Fig. 4 depend on the intensity distribution in the focal volume. For example, the quick rise of the band-head strengths below the characteristic change of slope indicates the increase of the laser peak intensity. At low pressure (left-hand panel), this increase slows down due to the depletion of neutral molecules in the central part of the focal volume [22, 24, 25]. It has been shown [22] that the same explanation does *not* hold at high pressures (right-hand panel), but here the deviation at a lower energy indicates that the peak intensity is clamped down to a maximum value near the characteristic change of slope, i.e., as the filamentation process sets in.

A comparison of the fluorescence spectra at low and high pressures allows for an estimation of the clamped peak intensity. From theoretical calculations [25] it is known that the depletion effect at low pressure (responsible for the change of slope) sets in at about  $2 \times 10^{14}$  W/cm<sup>2</sup> for the laser parameters of the current experiment. Since at atmospheric pressure the characteristic change of slope appears at a laser energy that is about four times smaller than that at low pressure, the clamped peak intensity is about  $5 \times 10^{13}$  W/cm<sup>2</sup>, in agreement with recent theoretical predictions [26].

The interpretation given above is also consistent with the results of numerical simulations using the parameters of the experimental setup in a pulse-propagation model [18, 22, 28]. In Fig. 5, results of the numerical calculations for the on-axis peak intensity in nitrogen molecular gas at 760 Torr are shown as a function of the distance from the lens at various input powers below and above the critical power for self-focusing. It is seen from the figure that the intensity distribution changes its shape from an undisturbed Gaussian distribution around the geometrical focus at low power to a broad distribution with a maximum before the geometrical focus and, finally, to a two-hump distribution indicating refocusing of the pulse. Most interesting here is that the increase in the maximum intensity is reduced for input powers near and above the critical power. This confirms the occurrence of intensity clamping in laser filaments at high gas pressure, as it was observed in the fluorescence measurements.

### 3.2. Intensity Clamping in Condensed Optical Media

In order to show that the phenomenon of intensity clamping is not limited to laser pulse filamentation in gases, but rather is a general phenomenon, a series of measurements of the supercontinuum spectrum generated by a Ti:sapphire laser pulse (800 nm, 170 fs) focused in different condensed media, namely, water, chloroform, and glass, has been performed. Different

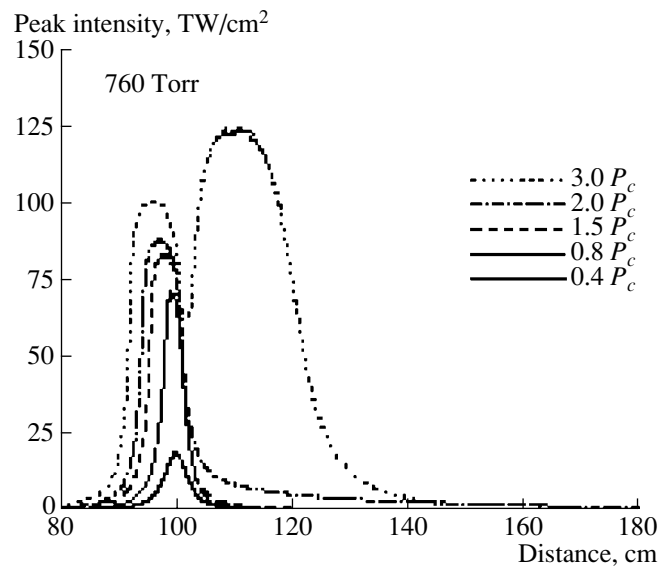


**Fig. 5.** Results of numerical simulations for the on-axis peak intensity as a function of the distance from the lens. The distributions are obtained for nitrogen molecular gas at different input pulse powers below and above the critical power for self-focusing,  $P_c$ , at 760 Torr.

setups have been used to filter out the strong central part of the pump pulse around 800 nm; for details, we refer to [27].

The spectra observed at various input laser powers in water are shown in Fig. 6 as a function of the wavelength, and results obtained at low input energies (left-hand panel) are compared with those obtained at high energies (right-hand panel). Each spectrum is normalized to unity at the central wavelength of 800 nm for the sake of comparison. At low input energies, we observe a symmetrical broadening of the spectrum to both sides of the central wavelength, whereas at the higher input energies a long pedestal on the blue side of the spectra appears up to a minimum wavelength of about 365 nm, which remains constant for an increase of the input energies by two orders of magnitude from 2 to 200  $\mu$ J. Similar observations have been made for chloroform and soda lime glass plate as well [27].

From simple qualitative theoretical considerations, it can be shown [27] that the frequency variation during pulse propagation mainly depends on changes in the temporal pulse form (e.g., self-steepening [18]) and on the plasma generation due to multiphoton ionization/excitation of the medium. Both are highly nonlinear effects that crucially depend on the peak intensity of the pulse. Thus, it has been argued [27] that the constant low-wavelength limit of the supercontinuum spectrum is an indication of a constant peak intensity inside the laser filaments. Thus, the phenomenon of intensity clamping in the filamentation of intense femtosecond laser pulses is found to occur not only in gases but also in various condensed optical media.

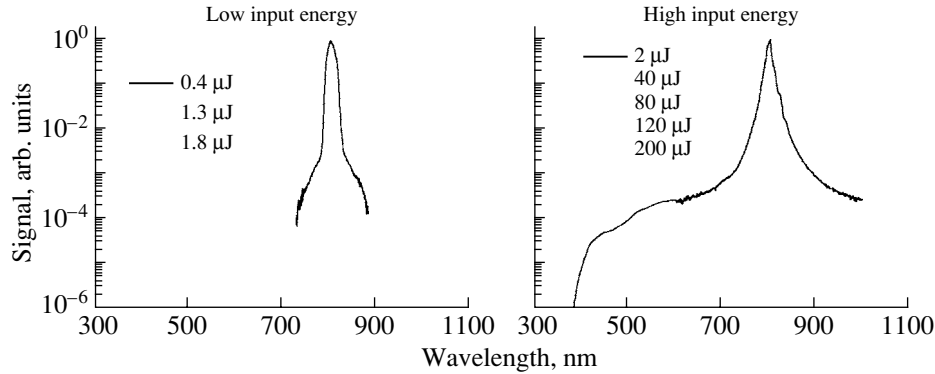


**Fig. 6.** Supercontinuum spectra obtained experimentally for propagation in water at various average input powers (see legends).

#### 4. TRANSVERSE-RING FORMATION

In another experiment [29], we exposed a silica glass plate in the filament in air at various propagation distances. A 350-fs laser pulse with energy 85 mJ was focused externally by a lens with a focal length of 150 cm. Damages on the plate were scanned by a Dek-TakII profilometer. This has allowed us to get a measure of the ablation profile, which is directly related to the distributed transverse fluence of the laser pulse. The experimental data are compared with the results of numerical simulations using initial conditions as close as possible to that of the experiment. To this end, we integrated Eq. (1) using the slowly varying envelope approximation ( $s = 0$ ). This was done because higher order correction terms do not contribute significantly to the propagation dynamics for the initial conditions considered here.

In Fig. 7 we exhibit the numerical results for the fluence distribution at different propagation distances, and the inset of each figure shows the experimental profile of the damage created at the surface of the glass plate [29]. Before the geometrical focal point, shown in panel (a), there is a central dip in the fluence profile, which is also observed in the experiment. Around the geometrical focal point (Fig. 7b), the dip in the fluence disappears and there is mainly a center part with an outer ring structure. This result is also in agreement with the experiment. Well beyond the geometrical focal point (Fig. 7c), we see that the outer ring structure has diminished, but we also see the reappearance of the dip in the fluence, which is also the case in the experiment. Thus, the numerical fluence distribution evolution as a function of propagation distance using similar experimental input conditions is in good qualitative agreement with the experiment.

#### 5. THIRD-HARMONIC GENERATION AND SELF-CHANNELING

The clamped peak intensity of about  $5 \times 10^{13}$  W/cm<sup>2</sup> in the laser filaments in air is sufficient to generate higher harmonics. The latter process is one of the fun-

damental nonlinear processes for laser frequency conversion and has wide application. In air, high conversion efficiencies of up to 0.1% have been observed [30, 31] for third-harmonic generation. We have shown [31, 32] both theoretically and experimentally that, during laser pulse filamentation in air, the fundamental- and the third-harmonic pulses form a two-colored filament due to a nonlinear phase-locking mechanism.

In both experiments and numerical calculations, the propagation of a linearly polarized, collimated Gaussian input laser pulse with a center wavelength at  $\lambda_0 = 800$  nm, a beam radius of  $w_0 = 0.3$  cm, and a pulse duration  $\tau_{\text{FWHM}} = 250$  fs has been investigated. The beam was focused with a lens with a focal length of  $f = 100$  cm in air. Our theoretical model is based on a set of coupled equations, which are written in dimensionless form in the retarded coordinate system ( $\tau = t - z/v_g(\omega)$ ) as [31]

$$i \frac{\partial \mathcal{E}_\omega}{\partial z} + \frac{1}{4} \nabla_\perp^2 \mathcal{E}_\omega - \frac{L_{DF}}{L_{PL}} N_e \mathcal{E}_\omega + \frac{L_{DF}}{L_{NL}} (|\mathcal{E}_\omega|^2 \mathcal{E}_\omega + \mathcal{E}_\omega^{*2} \mathcal{E}_{3\omega} + 2|\mathcal{E}_{3\omega}|^2 \mathcal{E}_\omega) = 0, \quad (3)$$

$$i \frac{\partial \mathcal{E}_{3\omega}}{\partial z} + \frac{1}{12} L_{\Delta k} \frac{\partial \mathcal{E}_{3\omega}}{\partial \tau} + \frac{L_{DF} \mathcal{E}_{3\omega}}{L_{\Delta k}} - \frac{L_{DF}}{3L_{PL}} N_e \mathcal{E}_{3\omega} + \frac{3L_{DF}}{L_{NL}} \left( |\mathcal{E}_{3\omega}|^2 \mathcal{E}_{3\omega} + \frac{\mathcal{E}_\omega^3}{3} + 2|\mathcal{E}_\omega|^2 \mathcal{E}_{3\omega} \right) = 0, \quad (4)$$

$$\frac{\partial N_e(\tau)}{\partial \tau} = (\Gamma_\omega (|\mathcal{E}_\omega|^2) + \Gamma_{3\omega} (|\mathcal{E}_{3\omega}|^2)) (1 - N_e(\tau)). \quad (5)$$

$\mathcal{E}_\omega$  and  $\mathcal{E}_{3\omega}$  are the electric-field envelope functions, normalized to the peak value of the input pump field  $\mathcal{E}_0 = \sqrt{2P_0/\pi w_0^2}$  and using the transformation  $\mathcal{E}_{3\omega} \rightarrow \mathcal{E}_{3\omega} e^{i\Delta k z}$ . The sub- and superscripts,  $\omega$  and  $3\omega$ , denote the fundamental- and third-harmonic pulses, respectively. The propagation direction  $z$  is scaled in units of

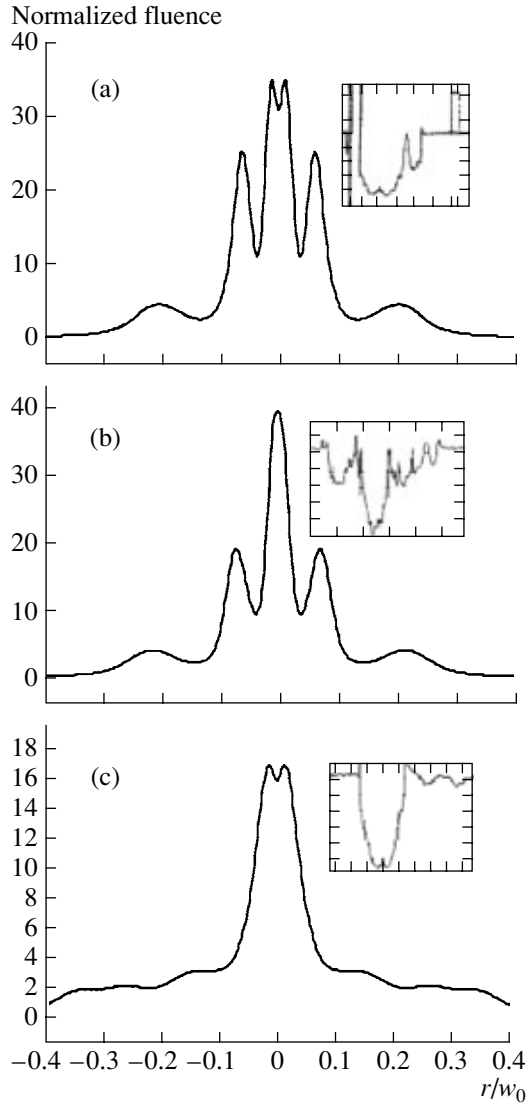


**Fig. 7.** The laser pulse fluence (normalized to the peak fluence) is plotted as a function of the radius at the positions (a) 59.5, (b) 60.5, and (c) 68 cm. Note the appearance of the dip in the center of the fluence profile, which disappears in (b) and reappears again in (c). Experimental results are shown in the insets.

$L_{DF} = k_{\omega} w_0^2 / 2$ , the temporal coordinate  $\tau$ , in units of the input pulse width  $\tau_0$ , and the transverse coordinate  $r$ , in units of the input beam radius  $w_0$ . Furthermore,  $L_{NL} = (n_2 k_{\omega} I_0)^{-1}$  is a nonlinear length scale, where  $I_0 = |\mathcal{E}_0|^2$ , and  $L_{PL} = k_{\omega} m_e c^2 / 2 \pi e^2 N_0$  is the plasma length scale, where  $N_0$  is the number density of neutral air molecules.  $L_{\Delta v} = (v_g^{-1}(3\omega) - v_g^{-1}(\omega))^{-1} \tau_0$  represents the characteristic temporal walk-off distance that is due to the group-velocity mismatch between the fundamental- and third-harmonic pulses. Finally,  $L_{\Delta k} = |\Delta k|^{-1} = |3k_{\omega} - k_{3\omega}|^{-1}$  is the linear wavevector mismatch length scale in the wavevectors  $k_{\omega} = n_{\omega} k_0$  and  $k_{3\omega} = n_{3\omega} k_0$ , where  $\Delta k =$

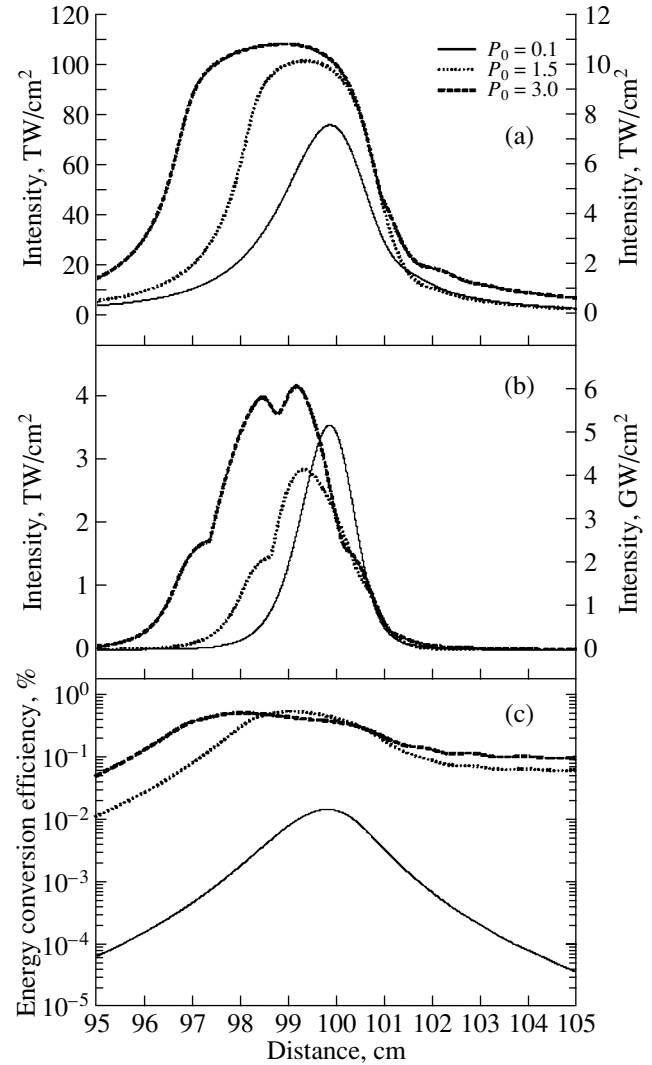


**Fig. 8.** Results of numerical calculations for the on-axis peak intensity of (a) the fundamental pulse and (b) the third-harmonic pulse at different input powers below and above the critical power for self-focusing as a function of the propagation distance; (c) total conversion efficiency as a function of the propagation distance.

$3k_0(n_{\omega} - n_{3\omega}) = -5.0 \text{ cm}^{-1}$ . Electron generation via multiphoton ionization of N<sub>2</sub> and O<sub>2</sub> by both pulses is taken into account using an S-matrix model formula [33]. The set of equations above is integrated numerically with the initial condition  $\mathcal{E}_{3\omega}(z=0) = 0$  for different input powers  $P_0$  both below and above the critical power  $P_{\text{crit}}$  for self-focusing and filamentation.

In Fig. 8, the numerical results for the on-axis peak intensity of the pump pulse (panel a) and the third harmonic pulse (panel b) are shown as a function of the propagation distance. In the linear focusing limit ( $P_0 = 0.1 P_{\text{crit}}$ , solid line), no distortion of the pump pulse occurs, and the pulse comes to a focus at the geometri-

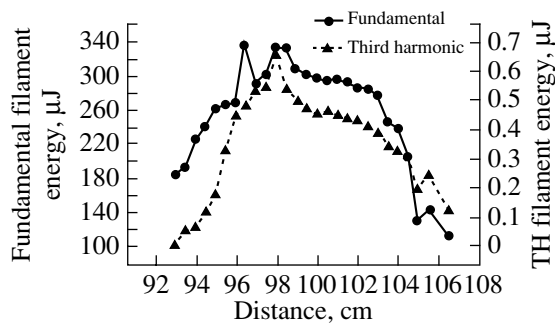


**Fig. 9.** Experimental data of the observation of the pump pulse (circles, left-hand scale) and the third-harmonic pulse (triangles, right hand scale) filament energy as a function of the propagation distance.

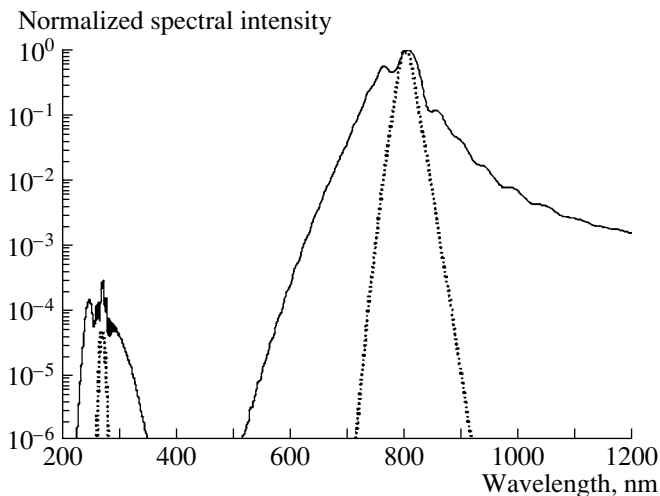


**Fig. 10.** Spectrum of the fundamental- and third-harmonic pulses before filamentation (dotted line) and in the filament (at  $z = 200$  cm, solid line). It can be seen that the third-harmonic pulse undergoes continuum generation and is red-shifted.

cal focus. As the input power is increased, the pump pulse self-focuses before the geometrical focus, and its peak intensity remains nearly unchanged over a distance of several centimeters, indicating filamentation of the pulse. The same filamentation phenomenon occurs for the third-harmonic pulse as well (panel b). The results in Fig. 8c show that the third-harmonic energy-conversion efficiency is roughly constant over the length of the filament, which is much longer than the characteristic coherence length. In addition, there is no apparent temporal walk-off between the two pulses; i.e., the third-harmonic pulse travels inside the filament with nearly the same group velocity as the fundamental pulse. It has been shown [31] that, inside the filament, the two pulses are coupled together in a quasi-steady-state condition with constant phase difference, thus forming a two-colored filament. Furthermore, the third-

harmonic pulse does not give back its energy to the pump pulse, even well after the filament has ceased.

The theoretical predictions are confirmed by a measurement [31] of the pump and the third-harmonic energies (defined as the values contained within the 400- $\mu\text{m}$  diameter of a pinhole placed at various positions along the filament). The experimental data, presented as a function of the propagation distance after the lens in Fig. 9, show that the pump pulse energy (circles, left-hand scale) and the third-harmonic pulse energy (triangles, right-hand scale) remain constant over the whole length of the filament.

It has been found [32] that the cofilamentation effect is rather independent of the wavelength of the input beam and the focal geometry. During the filamentation process, the third-harmonic pulse itself generates a broad continuum, as can be seen from the supercontinuum spectrum presented in Fig. 10 (solid line). For the sake of comparison, we have also plotted, by dotted lines, the respective fundamental pulse and the third-harmonic pulse just before the filamentation process starts. A comparison reveals that both the pulses are broadened during the filamentation process. This might potentially extend, in long-range femtosecond-pulse propagation, the effective spectral region of atmospheric sensing methods further into the UV and, hence, into an important wavelength regime for monitoring chemical pollutants and biological species.

## 6. SUMMARY

In conclusion, we have shown the complex and rich nonlinear propagation and interaction dynamics of high-peak-power femtosecond laser pulses in transparent optical media. It is shown that a generalized nonlinear envelope equation that includes higher order effects such as self-steepening adequately describes the propagation of high-power femtosecond laser pulses in optical media. Particularly, the self-steepening of the pulse, which forms a shock at the trailing part of the pulse, contributes significantly to the blueshift of the continuum generation and therefore cannot be neglected. We have also shown experimentally that, in all kinds of optical media matter, the peak pulse intensity inside the filament is clamped to a maximum value. This supports the fact that intensity clamping is a universal phenomenon. Finally, the generation of an intense ultra-short third-harmonic pulse during filamentation of the pump pulse has been investigated. The strong interaction of the two pulses results in a two-colored filament in which the third-harmonic pulse also undergoes continuum generation. This provides the possibility of extending the broadband spectrum well into the UV and could have potential applications in remote-sensing types of applications.

## ACKNOWLEDGMENTS

It is our pleasure to acknowledge the participation of Dr. A. Iwasaki, W. Liu, E. Oral, Dr. S. Petit, Dr. M. Scallora, Dr. A. Talebpour and Dr. K. Vijayalakshmi. This work has been partially by the following organizations: NSERC, DRDC-Valcartier, Canada Research Chair, CIPI, FQRNT, the Alexander von Humboldt Foundation, NATO, ARO, and DARPA.

## REFERENCES

1. Y. R. Shen, *The Principles of Nonlinear Optics* (Wiley, New York, 1984; Nauka, Moscow, 1989).
2. R. W. Boyd, *Nonlinear Optics* (Academic, Boston, 1992).
3. J. H. Marburger, *Prog. Quantum Electron.* **4**, 35 (1975).
4. A. Braun, G. Korn, X. Liu, *et al.*, *Opt. Lett.* **20**, 73 (1995).
5. A. Brodeur and S. L. Chin, *Phys. Rev. Lett.* **80**, 4406 (1998).
6. A. Brodeur, C. Y. Chien, F. A. Ilkov, *et al.*, *Opt. Lett.* **22**, 304 (1997).
7. M. Mlejnek, E. M. Wright, and J. V. Moloney, *Opt. Lett.* **23**, 382 (1998).
8. W. J. Jones and B. P. Stoicheff, *Phys. Rev. Lett.* **80**, 657 (1964).
9. P. B. Corkum, C. Rolland, and T. Srinivasan-Rao, *Phys. Rev. Lett.* **57**, 2268 (1986).
10. L. Wöste, C. Wedekind, H. Wille, *et al.*, *Laser Optoelectron.* **29**, 51 (1997).
11. *The Supercontinuum Laser Source*, Ed. by R. R. Alfano (Springer, New York, 1989).
12. S. L. Chin, A. Brodeur, S. Petit, *et al.*, *J. Nonlinear Opt. Phys. Mater.* **8**, 121 (1999).
13. V. P. Kandidov, O. G. Kosareva, I. S. Golubtsov, *et al.*, *Appl. Phys. B* **77**, 149 (2003).
14. K. R. Wilson and V. V. Yakovlev, *J. Opt. Soc. Am. B* **14**, 444 (1997).
15. X. M. Zhao, J.-C. Diels, C. V. Wang, and J. M. Elizondo, *IEEE J. Quantum Electron.* **31**, 599 (1995).
16. S. L. Chin and K. Miyazaki, *J. Appl. Phys.* **38**, 2011 (1999).
17. J. Kasparian, M. Rodriguez, G. Mejean, *et al.*, *Science* **301**, 61 (2003).
18. N. Aközbek, C. M. Bowden, and S. L. Chin, *Opt. Commun.* **191**, 353 (2001).
19. T. Brabec and F. Krausz, *Rev. Mod. Phys.* **72**, 545 (2000).
20. *CRC Handbook of Chemistry and Physics*, Ed. by D. R. Lide, 74th ed. (CRC Press, Boca Raton, FL, 1993), pp. 10–304.
21. E. T. J. Nibbering, G. Grillion, M. A. Franco, *et al.*, *J. Opt. Soc. Am. B* **14**, 650 (1997).
22. A. Becker, N. Aközbek, K. Vijayalakshmi, *et al.*, *Appl. Phys. B* **73**, 287 (2001).
23. A. Talebpour, S. Petit, and S. L. Chin, *Opt. Commun.* **171**, 285 (1999).
24. A. Talebpour, M. Abdel-Fattah, and S. L. Chin, *Opt. Commun.* **183**, 479 (2000).
25. A. Becker, A. D. Bandrauk, and S. L. Chin, *Chem. Phys. Lett.* **343**, 345 (2001).
26. J. Kasparian, R. Sauerbrey, and S. L. Chin, *Appl. Phys. B* **71**, 877 (2000).
27. W. Liu, S. Petit, A. Becker, *et al.*, *Opt. Commun.* **202**, 189 (2002).
28. N. Aközbek, C. M. Bowden, A. Talebpour, and S. L. Chin, *Phys. Rev. E* **61**, 4540 (2000).
29. S. L. Chin, N. Aközbek, A. Proulx, *et al.*, *Opt. Commun.* **188**, 181 (2001).
30. S. Backus, J. Peatross, Z. Zeek, *et al.*, *Opt. Lett.* **21**, 665 (1996).
31. N. Aközbek, A. Iwasaki, A. Becker, *et al.*, *Phys. Rev. Lett.* **89**, 143901 (2002).
32. N. Aközbek, A. Becker, M. Scallora, *et al.*, *Appl. Phys. B* **77**, 177 (2003).
33. J. Muth-Böhm, A. Becker, and F. H. M. Faisal, *Phys. Rev. Lett.* **85**, 2280 (2000).